LANGMUIR

pubs.acs.org/Langmuir Article

Iron, Nitrogen-Doped Carbon Aerogels for Fluorescent and Electrochemical Dual-Mode Detection of Glucose

Xingzi Wu,‖ Yujie Sun,‖ Ting He, Yulin Zhang,* Guo-Jun Zhang,* Qiming Liu, and Shaowei Chen*

Cite This: *Langmuir* 2021, 37, 11309−11315 Read Online

ACCESS | Metrics & More | Article Recommendations | Supporting Information

ABSTRACT: Due to their effective catalytic activity and maximum atom utilization, single metal atoms dispersed in carbon matrices have found diverse applications in electrocatalysis, photocatalysis, organic catalysis, and biosensing. Herein, iron is atomically dispersed into nitrogen-doped porous carbon aerogel by a facile pyrolysis procedure, and the resulting nanocomposite behaves both as a peroxidase mimic for the sensitive detection of glucose by fluorescence spectroscopy and as an effective catalyst for the electrochemical oxidation of glucose. The glucose concentration can be quantified within the millimolar to micromolar range with a limit of detection of 3.1 and 0.5 μM, respectively. Such a dual-functional detection platform also shows excellent reproducibility, stability, and selectivity, and the performance in glucose detection of clinical and artificial human body fluids is highly comparable to that of leading assays in recent studies and results from commercial sensors. Results from this study suggest that carbon aerogel-supported single atoms can be used as a dual-functional nanozyme for the construction of low-cost, high-performance dual-signal readout platforms for glucose detection.

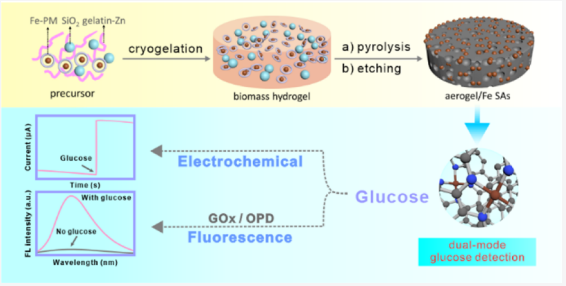

INTRODUCTION

Functional nanomaterial-based nanozymes have been attracting extensive interest, owing to their catalytic activity that is similar to native enzymes, yet with robust stability in harsh environments, ease of large-scale production, and low cost.[1] In fact, nanozymes have found diverse applications in biosensing,[2] therapeutics,[3] organic degradation,[4] and so on. Among these, nanozymes based on carbon nanomaterials,[5] transition metal nanomaterials,[6] nucleic acid-doped nanomaterials,[7] and noble metal nanomaterials[8,9] have been widely applied for disease diagnosis due to their unique selective activity toward disease-related substrates.[10] Glucose plays a critical role in the natural growth of cells, and disordered blood sugar levels are strongly correlated to diabetes.[11] Accurate monitoring of blood glucose concentration is one of the best ways to prevent and treat diabetes. Thus far, numerous analytical methods have been developed for the detection of glucose, including electrochemistry,[12] colorimetry,[13] fluorescence,[11] and chemiluminescence.[14] However, these methods are generally based on a single-signal readout mode,[15,16] and the accuracy of the detection may be compromised by external interferences, such as nonstandard test procedures, diverse surrounding environments, and even different operators. To address this challenge, multi-mode detection of analytes based on, for instance, electrochemistry and optical techniques is strongly desired.

Electrochemical bioanalysis has become a focus of research for glucose detection in recent years with high sensitivity and short response time. Yet, for the conventional enzyme-mediated glucose sensors, several drawbacks are commonly observed. For instance, the enzyme activity can be significantly affected by environmental variations, such as temperature, humidity, and pH. Hence, to mitigate such issues, development of non-enzymatic glucose sensors with high sensitivity, good stability, and low cost has emerged as an attractive strategy.

Fluorescence-based methods possess unique advantages, such as rapid analysis and excellent sensitivity.[11] In recent years, nanozymes mimicking glucose oxidase (GOx) and horseradish peroxidase (HRP) have been attracting extensive interest for glucose sensing and detection; yet, most of these nanozymes have to work under acidic conditions (pH = 3.0−5.0).[6,8,9] This greatly limits their applications in clinic tests under physiological conditions. In addition, most nanozymes require the use of noble metals.[17] Therefore, for both fundamental research and biomedical diagnosis, it is imperative to develop effective nanozymes with good sensitivity, selectivity, and low cost,[18] where both electrochemical and fluorescent platforms can be exploited for the dual-mode detection of glucose, so as to enhance the accuracy and minimize systematic and/or background errors.

Received: July 13, 2021
Revised: September 4, 2021
Published: September 19, 2021

https://doi.org/10.1021/acs.langmuir.1c01866
Langmuir 2021, 37, 11309−11315

In recent years, single-atom catalysts (SACs) have emerged as a unique system for the development of nanozymes due to their maximum atom utilization efficiency, unique geometry, and full exposure of active sites.[19] To mitigate the issues of migration and aggregation of the metal centers in SACs,[20] the metal loadings are typically maintained at a low level and the metal centers are embedded within a supporting matrix with strong chelating moieties, such as heteroatom (e.g., N, P, S, O, and B)-doped carbon.[21] Generally, increasing the loading of nitrogen and metal atoms is an ideal solution to enhance the activity of nanozymes, which can be achieved by increasing the defect density or metal concentration and/or choosing appropriate supports.[22] Hierarchical 3D N-doped porous carbon aerogels have been found to serve as a promising support matrix for SACs with their large surface area, rich mass transport channels, abundant reserves, and low cost.[23,24] Notably, Fe-based SACs have demonstrated excellent peroxidase-like activity and can catalyze the oxidation of molecular probes in the presence of hydrogen peroxide produced by the oxidation of glucose with GOx, as manifested in fluorescence spectroscopic measurements.[25] In electrochemical measurements, such Fe-based nanocomposites have also been found to catalyze the direct oxidation of glucose.[26] These unique properties may be exploited for the development of a dual-signal-detection platform.

In this study, a dual-functional single-iron atom nanozyme was prepared by embedding Fe single atoms in biomass-derived, 3D porous N-doped carbon aerogels (NCAG/Fe) and used for glucose detection based on a fluorescence and electrochemical dual-signal readout platform. The nanozyme showed robust peroxidase-like properties under physiological conditions, whereby nonfluorescent *o*-phenylenediamine (OPD) was oxidized to fluorescent 2,3-diaminophenazine (DAP) in the presence of H_2O_2 generated by GOx-catalyzed oxidation of glucose. Electrochemically, the NCAG/Fe nanocomposite also demonstrated an apparent electrocatalytic activity toward the oxidation of glucose. In such a dual-mode readout platform, the limit of detection (LOD) was estimated to be 3.1 μM in fluorometric assay and 0.5 μM in electrochemical detection. The detection platform also exhibited excellent reproducibility, stability, and selectivity; and the performance of glucose detection in clinical and artificial human body fluids was superior/comparable to that of leading assays in recent studies and results obtained from commercial sensors.

EXPERIMENTAL SECTION

Chemicals. Hydrogen peroxide (H_2O_2, 30%, w/w), disodium hydrogen phosphate (Na_2HPO_4), anhydrous calcium chloride ($CaCl_2$), potassium chloride (KCl), sodium chloride (NaCl), ascorbic acid (AA), urea, and OPD were obtained from Sinopharm Chemical Reagents Co., Ltd. (Shanghai, China). Gelatin, iron(II) chloride tetrahydrate ($FeCl_2{\cdot}4H_2O$), zinc(II) acetate dihydrate ($Zn(Ac)_2{\cdot}2H_2O$), SiO_2 nanoparticles, glucose, maltose, sucrose, fructose, and glycine were all purchased from Aladdin Reagents (Shanghai, China). GOx (100 U mg^{-1}, type X-S, from *Aspergillus niger*), 1,10-phenanthroline (PM) monohydrate, sodium hydroxide (NaOH), ammonium chloride (NH_4Cl), uric acid (UA), dopamine, L-lactic acid, L-histidine, L-glutamic acid, and lactose were purchased from Sigma-Aldrich. All other reagents were of analytical grade. Water was provided by a Millipore water purification system (18.2 MΩ cm). Serum samples were obtained from healthy volunteers in Wuhan No. 1 Hospital (Wuhan, China).

Preparation of Carbon Aerogels. The NCAG/Fe sample was prepared by adopting a procedure reported previously.[27−29] In brief, 24 mg of PM was dispersed in 200 μL of 0.2 M $FeCl_2{\cdot}4H_2O$ in water under sonication to produce a red $Fe(PM)_3^{2+}$ solution. Separately, 60 mg of gelatin, 30 mg of SiO_2 nanoparticles, and 2.7 mL of water were added in a screw-capped vial and mixed under magnetic stirring in a 60 °C water bath for 10 min, into which were then added 200 μL of the above prepared 0.2 M $Fe(PM)_3^{2+}$ and 80 μL of 1.0 M $Zn(Ac)_2$. The obtained hydrogels were subjected to freezing−thawing three times (denoted as G_{Si-Zn}/Fe-PM), before being pyrolyzed at 900 °C for 3 h in a tube furnace under a constant flow of 97% Ar + 3% H_2 at a heating rate of 5 °C min^{-1}. After being naturally cooled down to room temperature, the product was etched with HF to remove SiO_2 nanoparticles, affording NCAG/Fe.

Fe-free NCAG was prepared in the same fashion except for the addition of $FeCl_2$.

Characterization. The sample morphologies were examined by scanning electron microscopy (SEM, Hitachi S-4800) and transmission electron microscopy (TEM, FEI Talos F200S) measurements. Inductively coupled plasma-optical emission spectroscopy (ICP-OES) analysis was performed with a SPECTRO BLUE SOP instrument. X-ray diffraction (XRD) patterns were collected with a D/max 2550 X-ray power diffractometer. X-ray photoelectron spectroscopy (XPS) measurements were performed with an ESCALAB 250Xi instrument. Fluorescence tests were conducted using a Hitachi F-4600 fluorescence spectrophotometer. Nitrogen adsorption/desorption isotherms were acquired with a Micromeritics ASAP2460 instrument. X-ray absorption spectroscopy measurements were performed at the Shanghai Synchrotron Radiation Facility in the fluorescence mode at room temperature (298 K).

Fluorescence Assay for Glucose Detection. The steady-state kinetic measurements were performed by recording the absorbance at 415 nm at a 30 s interval within 1 min, and the apparent kinetic parameters were calculated based on the equation $\nu = \nu_{max}[S]/(K_m + [S])$, where ν is the initial reaction rate, ν_{max} is the maximum reaction rate, $[S]$ is the substrate (H_2O_2 or OPD) concentration, and K_m is the Michaelis−Menten constant.

For the detection of glucose, 10 μL of GOx (12 μg/mL) and 10 μL of glucose at various concentrations in 50 μL of a phosphate buffer (pH 7.4) were incubated at 37 °C for 40 min, into which were then added NCAG/Fe and OPD with a final concentration of 10 and 20 μg/mL, respectively. The mixture was further incubated for 10 min at 25 °C, and the fluorescence spectra were acquired under 414 nm excitation. All fluorescence measurements were repeated three times for the calculation of the standard deviation.

Non-Enzymatic Electrochemical Assay for Glucose Detection. In a typical experiment, 1 mg of the as-synthesized NCAG/Fe powders was suspended in a 1 mL solution that contained 475 μL of H_2O, 475 μL of ethanol, and 50 μL of a 5% Nafion solution. 10 μL of the produced ink was dropcast on the surface of a clean glassy carbon electrode (GCE, 3 mm in diameter) and dried in air. The modified GCE was used as the working electrode, a saturated calomel electrode as the reference electrode, and a platinum wire as the auxiliary electrode. All electrochemical measurements were performed with a CHI 440 electrochemical workstation. Chronoamperometry was performed at an applied potential of +0.35 V in a 0.1 M NaOH aqueous solution with glucose at various concentrations. The test of each sample was repeated three times, from which the standard deviation was estimated.

Detection of Glucose in Clinical and Artificial Samples. To detect glucose in human serum, methanol was mixed with blood samples to remove proteins under agitation for 2 min. The blood samples were then centrifuged at 10,000 rpm for 10 min, and the obtained supernatant was used for glucose detection.

Artificial saliva was prepared from Na_2HPO_4, $CaCl_2$, KCl, NaCl, and urea.[30] Artificial sweat was formulated using a solution containing 0.13 M NaCl, 0.01 M KCl, 0.02 M urea, and 0.01 M L-lactic acid.[31] Glucose solutions at various concentrations were then added to the artificial saliva and artificial sweat for glucose detection.

https://doi.org/10.1021/acs.langmuir.1c01866
Langmuir 2021, 37, 11309−11315

RESULTS AND DISCUSSION

Preparation and Characterization of NCAG/Fe. Figure 1a illustrates the fabrication procedure of the biomass-derived

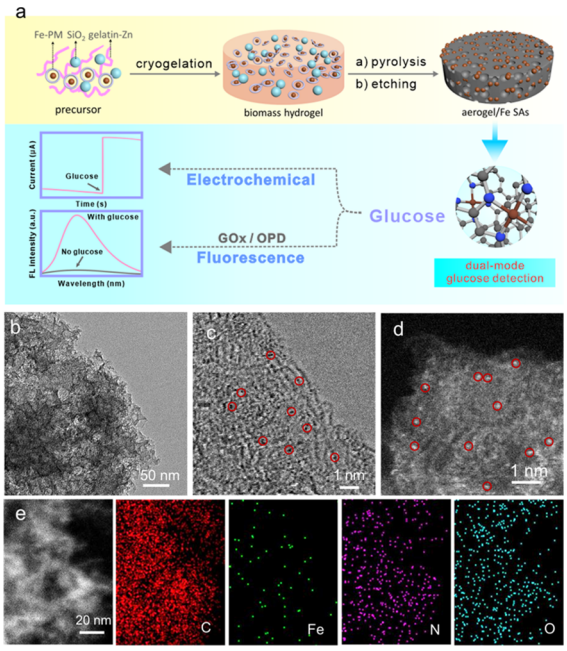

Figure 1. (a) Fabrication procedure of biomass-derived NCAG/Fe carbon aerogel, with the corresponding (b) TEM, (c) bright-field and (d) dark-field STEM images, and (e) elemental maps.

NCAG/Fe carbon aerogel, which entails three major steps:[27−29] (a) preparation of a gelatin−zinc hydrogel containing the $Fe(PM)_3^{2+}$ complex and SiO_2 nanoparticles by a repeated cryogelation process at −20 °C, where the SiO_2 nanoparticles were used as the structural templates, (b) controlled pyrolysis, and (c) acid etching for the transformation of the biomass hydrogel to N-doped carbon aerogel anchored with Fe single atoms (NCAG/Fe). As shown in Figure S1, the lyophilized hydrogel can be seen to exhibit a 3D honeycomb-like structure. After pyrolysis and HF etching, the hydrogel was converted to carbon aerogels with abundant mesopores, as manifested in TEM measurements (Figure 1b). In addition, a number of isolated dark (white) dots can be readily identified in the bright-field (dark-field) scanning TEM (STEM) images (red circles, Figure 1c,d), and the absence of nanoparticulate structures suggests that Fe was most likely atomically dispersed into the porous carbon framework. This is consistent with results from the corresponding elemental mapping analysis (Figure 1e).

Further structural insights of the as-synthesized NCAG/Fe carbon aerogel were obtained from N_2 adsorption−desorption isotherm, XRD, ICP-OES, and XPS measurements. From the N_2 adsorption−desorption isotherm and the corresponding pore size distribution (Figure S2 and inset), the NCAG/Fe aerogels can be found to possess a hierarchical pore structure with a high surface area of 1039.9 m^2 g^{-1}. From the XRD patterns in Figure 2a, NCAG/Fe can be seen to display only two broad diffraction peaks at 2θ = 24.2 and 43.5° due to the (002) and (101) planes of the partially graphitized carbon, respectively (PDF 656212).[27−29] The fact that no other diffraction peaks can be observed further confirms the absence of metal (oxide) nanoparticles in the sample, consistent with

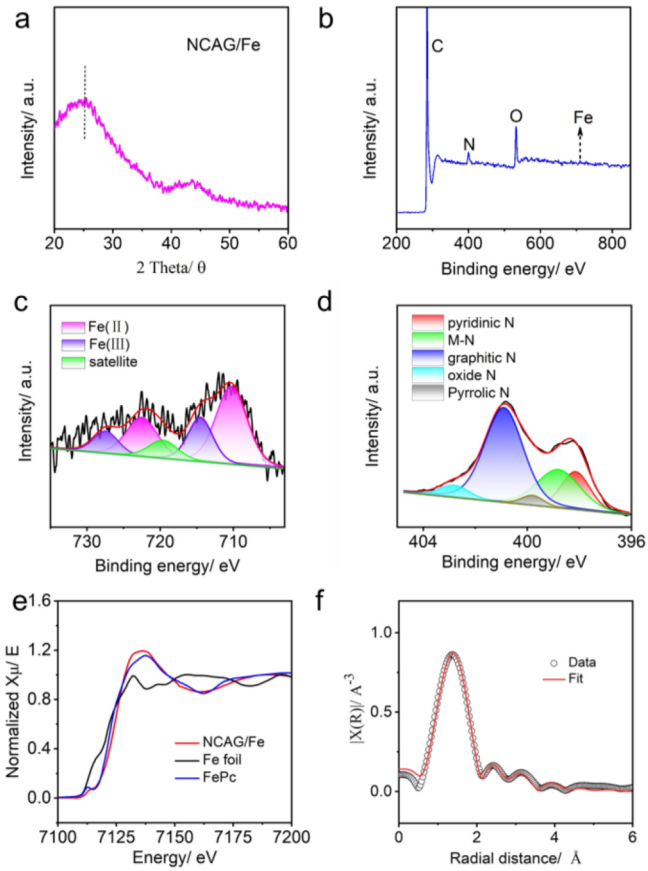

Figure 2. (a) XRD patterns of NCAG/Fe. (b) XPS survey spectrum and high-resolution scans of the (c) Fe 2p and (d) N 1s electrons of NCAG/Fe. Black curves in panel (c,d) are the experimental data and colored peaks are deconvolution fits. (e) Fe K-edge XANES spectra of NCAG/Fe, Fe foil, and FePc. (f) EXAFS spectrum and the corresponding fit of NCAG/Fe.

results from TEM measurements where Fe was atomically dispersed within the carbon aerogel (Figure 1).

The elemental compositions of the NCAG/Fe carbon aerogel were then quantitatively analyzed by XPS measurements. From the XPS survey spectrum in Figure 2b, the elements of C, N, O, and Fe can be readily identified at ca. 285, 400, 531, and 715 eV, respectively; and based on the integrated peak areas, the elemental composition was quantified at 87.35 wt % for C, 7.72 wt % for O, 3.99 wt % for N, and 0.95 wt % for Fe (Table S1). Note that the Fe content was in good agreement with that obtained from ICP-OES analysis (0.70 wt % Fe). The high-resolution scan of the Fe 2p electrons is depicted in Figure 2c, where two doublets can be deconvoluted at 710.3/722.5 and 714.5/727.4 eV due to the $2p_{1/2}$ and $2p_{3/2}$ electrons of Fe(II) and Fe(III), respectively.[29,32] Figure 2d shows the corresponding N 1s spectrum, where five species were resolved, pyridinic N at 398.2 eV, Fe−N at 398.8 eV, pyrrolic N at 399.8 eV, graphitic N at 400.9 eV, and oxide N at 402.5 eV.[29,32] Notably, in the O 1s spectrum (Figure S3), no Fe−O peak (ca. 530 eV) was resolved, confirming that indeed no iron oxides were formed in the sample and the Fe centers were most likely coordinated with the N dopants, rather than O, in the carbon matrix. Furthermore, as listed in Tables S1 and S2, the NCAG/Fe carbon aerogel contained 0.83 at % N in Fe−N and 0.21 at % Fe, corresponding to a Fe:N atomic

https://doi.org/10.1021/acs.langmuir.1c01866
Langmuir 2021, 37, 11309−11315

ratio of 1:3.95, that is, FeN_4 single-atom moieties were most likely formed within the NCAG/Fe carbon aerogel.

The atomic configuration of the metal sites was then investigated by X-ray absorption near-edge structure (XANES) and extended X-ray absorption fine structure (EXAFS) measurements. From Figure 2e, one can see that the Fe K-edge of NCAG/Fe is close to that of iron(II) phthalocyanine (FePc) but greatly different from that of Fe foil, suggesting a similar chemical state of NCAG/Fe and FePc. Yet, one can see that the absorption edge of NCAG/Fe was about 0.8 eV higher than that of FePc, suggesting a valence state between +2 and +3. In addition, the pre-edge peak of NCAG/Fe can be seen to be somewhat weaker than that of FePc (with an in-plane metal-N_4 site), indicating the formation of out-of-plane metal sites in the carbon aerogel. The corresponding EXAFS spectrum of NCAG/Fe shows only one peak at 1.4 Å, which is assigned to metal-N species (Figure 2f). From the fitting results of the EXAFS data (Figures 2f and S4, Table S3), the Fe−N coordination number was estimated to be 4.0, suggesting the formation of FeN_4 moieties in the porous carbon aerogel, in good agreement with results from XPS measurements (Table S2).

Results from our previous work[33] have shown that the catalytic performance was contingent upon the single-atom loading, and the NCAG/Fe sample with 0.95 wt % Fe (Table S1) represented the optimal loading. This is why it was chosen for the present study.

Quantitative Detection of Glucose by Fluorescence Spectroscopy. From Figure S5a, a prominent emission peak can be observed at 568 nm in a phosphate buffer solution (pH 7.4) containing 20 μg/mL OPD, 1 mM H_2O_2, and 10 μg/mL NCAG/Fe, characteristic of DAP produced from OPD oxidation.[6,8,9] Note that the emission was substantially reduced in the absence of H_2O_2, and no obvious emission was observed with only NCAG/Fe, OPD, NCAG + H_2O_2 + OPD, or OPD + H_2O_2 (Figure S5b). This suggests that NCAG/Fe indeed behaved as a peroxidase mimic that can catalyze the oxidation of OPD to DAP with H_2O_2.[6,8,9] Notably, as compared to the nanozymes reported previously which exhibit peroxidase-mimic activities under acidic conditions, the NCAG/Fe shows robust peroxidase-like properties under physiological conditions. This is attributed to the unique activity of NCAG/Fe in catalyzing the formation of hydroxyl radical (•OH) from H_2O_2, which then oxidized (nonfluorescent) OPD to (fluorescent) PAD. Such a property can be exploited as a unique platform for the detection of metabolites where hydrogen peroxide is catalytically produced.

We will first examine the detection of H_2O_2 based on NCAG/Fe before moving on to glucose as H_2O_2 can be readily generated by the oxidation of glucose catalyzed by GOx.[34] Peroxidase-like activity is known to be dependent on many factors.[35,36] To achieve the best performance for H_2O_2 detection, various important parameters were optimized, such as the concentrations of NCAG/Fe and OPD, reaction time, temperature, and solution pH. Fluorescence response efficiency (F/F_0, where F and F_0 are the fluorescence intensities with and without H_2O_2, respectively) is generally used as a descriptor to select the optimal conditions. The concentrations of NCAG/Fe and OPD were first optimized. From Figure S6a,b, one can see that the F/F_0 reached the maximum at 10 μg/mL NCAG/Fe and 20 μg/mL OPD. Thus, in order to minimize interference of excessive enzymes and substrates, such concentrations were used in the subsequent experiments. Next, the impact of reaction time was examined, and from Figure S6c, the F/F_0 value can be seen to peak at ca. 10 min, signifying that 10 min was the optimal reaction time. Similarly, the optimal solution temperature was identified at 25 °C (Figure S6d) and optimal pH at 7.4 (Figure S7).

To better understand the peroxidase-mimicking catalytic activity of NCAG/Fe, steady-state kinetic measurements were carried out under neutral conditions. From the apparent K_m and v_{max} values shown in Table S4, the NCAG/Fe nanozyme can be seen to exhibit an affinity and catalytic activity toward the two substrates under neutral conditions comparable to that of HRP but in acidic solutions.

Under the optimized experimental conditions identified above, the fluorescence emission spectra were acquired with NCAG/Fe (10 μg/mL), OPD (20 μg/mL), and H_2O_2 at varying concentrations. As illustrated in Figure S8a, the fluorescence emission at 568 nm became intensified with increasing concentration of H_2O_2 from 0.01 to 20 mM (Figure S8b), exhibiting a good linear relationship in the range of 0.01−1 mM (F/F_0 = 4.8177[H_2O_2] + 0.9948, with R^2 = 0.9968, Figure S8c). The detection limit ($3\sigma/k$, with k being the slope of the curve and σ the standard deviation) was as low as 1.8 μM. Such a sensitive detection of H_2O_2 based on NCAG/Fe carbon aerogel makes it possible to extend the sensor system for glucose detection, where the optimal GOx concentration was identified at 12 μg/mL (Figure S9a) and incubation time at 40 min (Figure S9b).

Under these optimal conditions, the fluorescence emission spectra at 414 nm excitation were acquired with the solution containing GOx (12 μg/mL), NCAG/Fe (10 μg/mL), OPD (20 μg/mL), and glucose at different concentrations (Figure 3a). It can be observed that with the increasing glucose concentration, the fluorescence intensity at 568 nm increased accordingly. Figure 3b shows the corresponding F/F_0, which

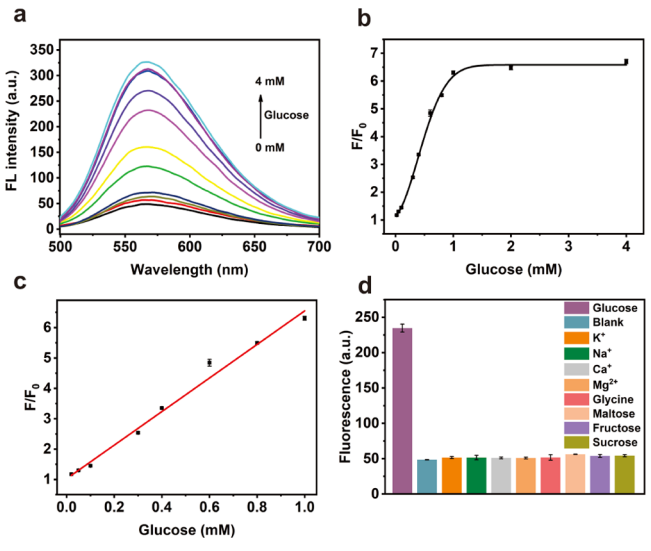

Figure 3. (a) Fluorescence emission spectra at 414 nm excitation with the solution containing GOx (12 μg/mL), NCAG/Fe (10 μg/mL), OPD (20 μg/mL), and glucose at different concentrations (specified in figure legends). (b) Fluorescence response efficiency (F/F_0) *vs* glucose concentration. (c) Linear range (calibration curve) for the detection of glucose. (d) Fluorescence response in the presence of different saccharides, metal ions, and amino acids (3 mM each). The concentration of glucose is 0.6 mM. Error bars represent the standard deviations of three repetitive experiments.

https://doi.org/10.1021/acs.langmuir.1c01866
Langmuir 2021, 37, 11309−11315

features a linear range from 0.02 to 1 mM (Figure 3c) with the calibration curve expressed as F/F_0 = 5.5243[glucose] + 1.0274 (R^2 = 0.9932). The detection limit was estimated to be ca. 3.1 μM, which is comparable to leading results reported for relevant nanozyme-based glucose sensors (Table S5). It has been known that the blood glucose level of diabetics is usually ≥7 mM.[37] Thus, the NCAG/Fe-carbon aerogel may serve as a low-cost, high-performance platform for glucose detection, a critical step in diabetes diagnosis and monitoring.

In addition to high sensitivity, the NCAG/Fe-based sensing system also shows excellent selectivity toward glucose detection. From Figure 3d, one can see that only glucose results in a remarkable fluorescence response, while no obvious fluorescence signals were detected in the presence of a wide variety of potential interferents, such as fructose, maltose, sucrose, glycine, and common inorganic ions, even at a rather high concentration (3 mM). This clearly confirms the excellent selectivity of the NCAG/Fe-based sensing platform and its feasibility for glucose detection in clinical serum samples, which contain a range of interfering metabolites (vide infra). The superb selectivity of NCAG/Fe for distinguishing glucose from potential interferents is due to the substrate-specific catalysis of GOx.

Quantitative Detection of Glucose by Electrochemical Measurements. To demonstrate the application of NCAG/Fe for non-enzymatic glucose sensing, the nanocomposite was deposited on a GCE surface and examined by chronoamperometric measurements. From Figure S10, one can see that in comparison to the zero current response at the bare GCE, the (Fe-free) NCAG-modified electrode produced a small-current step, which was markedly enhanced with NCAG/Fe. This demonstrates that the FeN_4 moieties in NCAG/Fe were highly active in the electrocatalytic oxidation of glucose. At an optimal NaOH concentration of 0.1 M (Figure S11a) and an applied potential of 0.35 V (Figure S11b), the NCAG/Fe nanocomposite indeed shows an excellent activity toward glucose oxidation (Figure 4a), where a wide linear response was observed within the concentration range of 2−2000 μM, with the corresponding calibration equation of I (μA) = 0.004 [glucose] + 0.018 and a correlation coefficient (R^2) of 0.9976 (Figure 4b). In addition, the LOD was estimated to be 0.5 μM (S/N = 3), comparable to leading results reported in earlier studies based on relevant nanozyme-based glucose sensors (Table S5).

The electrochemical platform also exhibited remarkable specificity in glucose detection (Figure 4c). In comparison to the significant current response upon the addition of glucose, no obvious current signals were observed with a range of potential interference species, such as NH_4Cl, uric acid, lactose, dopamine, L-AA, L-glutamic acid, and L-histidine. This result highlights the excellent selectivity of NCAG/Fe toward glucose detection. The reproducibility and stability of NCAG/Fe-based electrochemical assay were also investigated. As shown in Figure S12, the chronoamperometric responses of five NCAG/Fe-modified electrodes produced very close results with a low relative standard deviation of only 0.94%, suggesting excellent reproducibility. In addition, Figure 4d shows the chronoamperometric responses of a NCAG/Fe-based electrode stored under ambient conditions for up to a week with the addition of 100 μM glucose, which exhibited a low current decay of only 8.7%, indicating excellent stability as well.

Detection of Glucose in Clinical and Artificial Samples. In order to verify the practicability of the NCAG/Fe-based dual-mode assay platform, further studies were carried out to detect glucose in actual clinical serum, artificial sweat, and artificial saliva samples. Pretreated serum samples were obtained from Wuhan No. 1 Hospital and diluted as needed. From the testing results in Table 1, it can be clearly seen that the results for the clinical serum samples detected using the NCAG/Fe-based dual-mode assay platform were consistent with those from a commercial glucometer, where the relative errors were in a narrow range of 2.8−5.4%. From Table 2, one can also see that the glucose concentration in artificial sweat and artificial saliva was accurately detected with a low relative error in a range of −4.5 to +4.4%. These results suggest that the NCAG/Fe-based dual-mode platform possesses the desired potential for clinical applications with complicated body fluids.

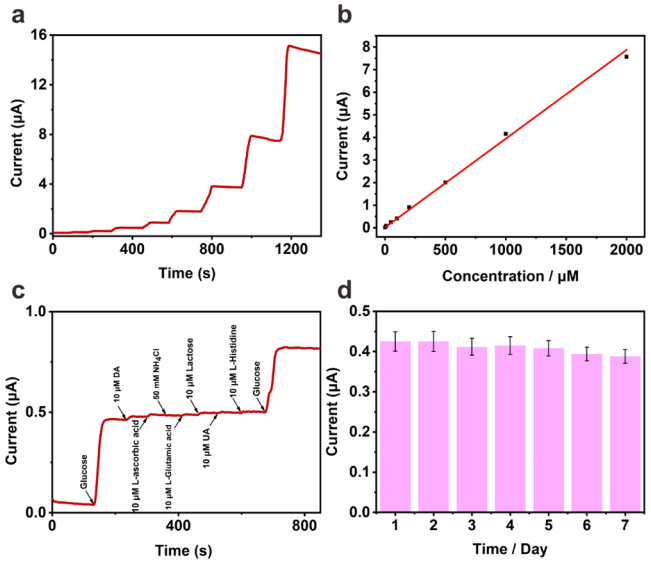

Figure 4. (a) Amperometric response of NCAG/Fe upon the addition of glucose at various concentrations (2, 10, 50, 100, 200, 500, 1000, and 2000 μM) to a 0.1 M NaOH solution at an applied potential of +0.35 V. (b) Corresponding linear correlation between the oxidation current increase and glucose concentration in the range of 2−2000 μM. (c) Chronoamperometric response of the NCAG/Fe electrode upon the addition of different interferents, dopamine, L-AA, NH_4Cl, L-glutamic acid, lactose, uric acid, and L-histidine. (d) Chronoamperometric profiles of the NCAG/Fe electrode stored under ambient conditions for up to a week with the addition of 100 μM glucose.

Table 1. Analysis of Glucose Contents in Human Serum Samples Using NCAG/Fe-Based Assay

sample	clinical data (mM)	fluorometric (mM)	relative error (%)	electrochemical (mM)	relative error (%)
1	4.3	4.42 ± 0.03	2.8	4.46 ± 0.08	3.7
2	4.6	4.79 ± 0.08	4.1	4.75 ± 0.05	3.3
3	5.5	5.72 ± 0.20	4.0	5.67 ± 0.03	3.1
4	5.7	6.01 ± 0.04	5.4	5.92 ± 0.10	3.9
5	6.1	6.43 ± 0.09	5.4	6.38 ± 0.09	4.6

CONCLUSIONS

In this study, carbon aerogels with atomically dispersed Fe were prepared by controlled pyrolysis of biomass precursors and served as an accurate and reliable dual-functional

https://doi.org/10.1021/acs.langmuir.1c01866
Langmuir 2021, 37, 11309−11315

Table 2. Analysis of Glucose Contents in Artificial Sweat and Saliva Samples Using the NCAG/Fe-Based Assay

sample	added glucose (μM)	fluorometric assay (μM)	relative error (%)	electrochemical assay (μM)	relative error (%)
sweat	60	57.29 ± 6.33	−4.5	62.44 ± 2.45	4.1
	80	82.75 ± 6.84	3.4	81.25 ± 2.55	1.6
	100	97.58 ± 2.09	−2.4	103.26 ± 2.89	3.3
saliva	30	30.10 ± 3.74	0.3	30.58 ± 2.08	1.9
	110	113.04 ± 3.67	2.8	114.86 ± 3.52	4.4
	190	191.39 ± 8.57	0.7	192.24 ± 6.76	1.2

nanozyme for the fluorescence and electrochemical detection of glucose. The unique activity was ascribed to the FeN_4 moieties embedded in the aerogel scaffold. The LOD was identified to be 3.1 μM in fluorometric assay and 0.5 μM in electrochemical assay. The NCAG/Fe-based sensing platform also demonstrated remarkable reproducibility, stability and selectivity and was used for the successful quantitative testing of glucose in clinical serum samples and artificial body fluids. Results from this study suggest that single atom-doped carbon aerogels may be exploited as a viable framework in the development of low-cost, high-performance, and high-selectivity nanozyme sensors for biomedical applications.

■ ASSOCIATED CONTENT

Supporting Information

The Supporting Information is available free of charge at https://pubs.acs.org/doi/10.1021/acs.langmuir.1c01866.

Additional SEM, XPS, EXAFS, fluorescence, and electrochemical data; nitrogen adsorption−desorption isotherm; summaries of elemental compositions, atomic configuration, and kinetic parameters; and comparison of detection performance with literature results (PDF)

■ AUTHOR INFORMATION

Corresponding Authors

Yulin Zhang − *School of Laboratory Medicine, Hubei University of Chinese Medicine, Wuhan, Hubei 430065, China*; Email: zhangyulin2001@163.com

Guo-Jun Zhang − *School of Laboratory Medicine, Hubei University of Chinese Medicine, Wuhan, Hubei 430065, China*; Email: zhanggj@hbtcm.edu.cn

Shaowei Chen − *Department of Chemistry and Biochemistry, University of California, Santa Cruz, California 95064, United States*; orcid.org/0000-0002-3668-8551; Email: shaowei@ucsc.edu

Authors

Xingzi Wu − *School of Laboratory Medicine, Hubei University of Chinese Medicine, Wuhan, Hubei 430065, China*

Yujie Sun − *School of Laboratory Medicine, Hubei University of Chinese Medicine, Wuhan, Hubei 430065, China*

Ting He − *School of Chemistry and Chemical Engineering, Central South University, Changsha, Hunan 410083, China*; orcid.org/0000-0003-2854-1645

Qiming Liu − *Department of Chemistry and Biochemistry, University of California, Santa Cruz, California 95064, United States*; orcid.org/0000-0001-5839-5453

Complete contact information is available at: https://pubs.acs.org/10.1021/acs.langmuir.1c01866

Author Contributions

[‖]X.W. and Y.S. authors contributed equally. The article was written through contributions of all authors. All authors have given approval to the final version of the article.

Notes

The authors declare no competing financial interest.

■ ACKNOWLEDGMENTS

S.W.C. thanks the National Science Foundation for partial support for the work (CHE-1900235 and CHE-2003685).

■ REFERENCES

(1) Huang, Y.; Ren, J.; Qu, X. Nanozymes: Classification, Catalytic Mechanisms, Activity Regulation, and Applications. *Chem. Rev.* **2019**, *119*, 4357−4412.

(2) Nandhakumar, P.; Kim, G.; Park, S.; Kim, S.; Kim, S.; Park, J. K.; Lee, N. S.; Yoon, Y. H.; Yang, H. Metal Nanozyme with Ester Hydrolysis Activity in the Presence of Ammonia-Borane and Its Use in a Sensitive Immunosensor. *Angew. Chem. Int. Ed.* **2020**, *59*, 22419−22422.

(3) Wang, Z.; Li, Z.; Sun, Z.; Wang, S.; Ali, Z.; Zhu, S.; Liu, S.; Ren, Q.; Sheng, F.; Wang, B.; Hou, Y. Visualization nanozyme based on tumor microenvironment "unlocking" for intensive combination therapy of breast cancer. *Sci. Adv.* **2020**, *6*, No. eabc8733.

(4) Li, S.; Hou, Y.; Chen, Q.; Zhang, X.; Cao, H.; Huang, Y. Promoting Active Sites in MOF-Derived Homobimetallic Hollow Nanocages as a High-Performance Multifunctional Nanozyme Catalyst for Biosensing and Organic Pollutant Degradation. *ACS Appl. Mater. Interfaces* **2020**, *12*, 2581−2590.

(5) Fan, K.; Xi, J.; Fan, L.; Wang, P.; Zhu, C.; Tang, Y.; Xu, X.; Liang, M.; Jiang, B.; Yan, X.; Gao, L. In vivo guiding nitrogen-doped carbon nanozyme for tumor catalytic therapy. *Nat. Commun.* **2018**, *9*, 1440.

(6) Jiao, L.; Wu, J.; Zhong, H.; Zhang, Y.; Xu, W.; Wu, Y.; Chen, Y.; Yan, H.; Zhang, Q.; Gu, W.; Gu, L.; Beckman, S. P.; Huang, L.; Zhu, C. Densely Isolated FeN4 Sites for Peroxidase Mimicking. *ACS Catal.* **2020**, *10*, 6422−6429.

(7) Du, Z.; Wei, C. Using G-Rich Sequence to Enhance the Peroxidase-Mimicking Activity of DNA-Cu/Ag Nanoclusters for Rapid Colorimetric Detection of Hydrogen Peroxide and Glucose. *ChemistrySelect* **2020**, *5*, 5166−5171.

(8) Deng, W.; Peng, Y.; Yang, H.; Tan, Y.; Ma, M.; Xie, Q.; Chen, S. Ruthenium Ion-Complexed Carbon Nitride Nanosheets with Peroxidase-like Activity as a Ratiometric Fluorescence Probe for the Detection of Hydrogen Peroxide and Glucose. *ACS Appl. Mater. Interfaces* **2019**, *11*, 29072−29077.

(9) Nie, F.; Ga, L.; Ai, J.; Wang, Y. Trimetallic PdCuAu Nanoparticles for Temperature Sensing and Fluorescence Detection of H2O2 and Glucose. *Front. Chem.* **2020**, *8*, 244.

(10) Rhee, S. G. CELL SIGNALING: H2O2, a Necessary Evil for Cell Signaling. *Science* **2006**, *312*, 1882−1883.

(11) Du, P.; Niu, Q.; Chen, J.; Chen, Y.; Zhao, J.; Lu, X. "Switch-On" Fluorescence Detection of Glucose with High Specificity and Sensitivity Based on Silver Nanoparticles Supported on Porphyrin Metal-Organic Frameworks. *Anal. Chem.* **2020**, *92*, 7980−7986.

(12) Zhang, X.; Luo, J.; Tang, P.; Morante, J. R.; Arbiol, J.; Xu, C.; Li, Q.; Fransaer, J. Ultrasensitive binder-free glucose sensors based on the pyrolysis of in situ grown Cu MOF. *Sens. Actuators, B* **2018**, *254*, 272−281.

(13) Liu, W.; Tian, J.; Mao, C.; Wang, Z.; Liu, J.; Dahlgren, R. A.; Zhang, L.; Wang, X. Sulfur vacancy promoted peroxidase-like activity of magnetic greigite (Fe3S4) for colorimetric detection of serum glucose. *Anal. Chim. Acta* **2020**, *1127*, 246−255.

(14) Shen, C.-L.; Zheng, G.-S.; Wu, M.-Y.; Wei, J.-Y.; Lou, Q.; Ye, Y.-L.; Liu, Z.-Y.; Zang, J.-H.; Dong, L.; Shan, C.-X. Chemiluminescent carbon nanodots as sensors for hydrogen peroxide and glucose. *Nanophotonics* **2020**, *9*, 3597−3604.

(15) Chen, M.; Zhou, H.; Liu, X.; Yuan, T.; Wang, W.; Zhao, C.; Zhao, Y.; Zhou, F.; Wang, X.; Xue, Z.; Yao, T.; Xiong, C.; Wu, Y. Single Iron Site Nanozyme for Ultrasensitive Glucose Detection. *Small* **2020**, *16*, No. e2002343.
(16) Xiong, C.; Tian, L.; Xiao, C.; Xue, Z.; Zhou, F.; Zhou, H.; Zhao, Y.; Chen, M.; Wang, Q.; Qu, Y.; Hu, Y.; Wang, W.; Zhang, Y.; Zhou, X.; Wang, Z.; Yin, P.; Mao, Y.; Yu, Z.-Q.; Cao, Y.; Duan, X.; Zheng, L.; Wu, Y. Construction of highly accessible single Co site catalyst for glucose detection. *Sci. Bull.* **2020**, *65*, 2100−2106.
(17) Huang, L.; Zhu, Q.; Zhu, J.; Luo, L.; Pu, S.; Zhang, W.; Zhu, W.; Sun, J.; Wang, J. Portable Colorimetric Detection of Mercury(II) Based on a Non-Noble Metal Nanozyme with Tunable Activity. *Inorg. Chem.* **2019**, *58*, 1638−1646.
(18) Sehit, E.; Altintas, Z. Significance of nanomaterials in electrochemical glucose sensors: An updated review (2016-2020). *Biosens. Bioelectron.* **2020**, *159*, 112165.
(19) Huang, L.; Chen, J.; Gan, L.; Wang, J.; Dong, S. Single-atom nanozymes. *Sci. Adv.* **2019**, *5*, No. eaav5490.
(20) Zhao, L.; Zhang, Y.; Huang, L.-B.; Liu, X.-Z.; Zhang, Q.-H.; He, C.; Wu, Z.-Y.; Zhang, L.-J.; Wu, J.; Yang, W.; Gu, L.; Hu, J.-S.; Wan, L.-J. Cascade anchoring strategy for general mass production of high-loading single-atomic metal-nitrogen catalysts. *Nat. Commun.* **2019**, *10*, 1278.
(21) Li, X.; Liu, L.; Ren, X.; Gao, J.; Huang, Y.; Liu, B. Microenvironment modulation of single-atom catalysts and their roles in electrochemical energy conversion. *Sci. Adv.* **2020**, *6*, No. eabb6833.
(22) Wang, J.; Li, Z.; Wu, Y.; Li, Y. Fabrication of Single-Atom Catalysts with Precise Structure and High Metal Loading. *Adv. Mater.* **2018**, *30*, 1801649.
(23) Fu, G.; Liu, Y.; Wu, Z.; Lee, J.-M. 3D Robust Carbon Aerogels Immobilized with Pd3Pb Nanoparticles for Oxygen Reduction Catalysis. *ACS Appl. Nano Mater.* **2018**, *1*, 1904−1911.
(24) Lv, Q.; Si, W.; He, J.; Sun, L.; Zhang, C.; Wang, N.; Yang, Z.; Li, X.; Wang, X.; Deng, W.; Long, Y.; Huang, C.; Li, Y. Selectively nitrogen-doped carbon materials as superior metal-free catalysts for oxygen reduction. *Nat. Commun.* **2018**, *9*, 3376.
(25) Zhang, R.; He, S.; Zhang, C.; Chen, W. Three-dimensional Fe- and N-incorporated carbon structures as peroxidase mimics for fluorescence detection of hydrogen peroxide and glucose. *J. Mater. Chem. B* **2015**, *3*, 4146−4154.
(26) Mei, H.; Wu, W.; Yu, B.; Wu, H.; Wang, S.; Xia, Q. Nonenzymatic electrochemical sensor based on Fe@Pt core-shell nanoparticles for hydrogen peroxide, glucose and formaldehyde. *Sens. Actuators, B* **2016**, *223*, 68−75.
(27) Chen, Y.; Hu, S.; Nichols, F.; Bridges, F.; Kan, S.; He, T.; Zhang, Y.; Chen, S. Carbon aerogels with atomic dispersion of binary iron-cobalt sites as effective oxygen catalysts for flexible zinc-air batteries. *J. Mater. Chem. A* **2020**, *8*, 11649−11655.
(28) He, T.; Zhang, Y.; Chen, Y.; Zhang, Z.; Wang, H.; Hu, Y.; Liu, M.; Pao, C.-W.; Chen, J.-L.; Chang, L. Y.; Sun, Z.; Xiang, J.; Zhang, Y.; Chen, S. Single iron atoms stabilized by microporous defects of biomass-derived carbon aerogels as high-performance cathode electrocatalysts for aluminum-air batteries. *J. Mater. Chem. A* **2019**, *7*, 20840−20846.
(29) He, T.; Lu, B. Z.; Chen, Y.; Wang, Y.; Zhang, Y. Q.; Davenport, J. L.; Chen, A. P.; Pao, C. W.; Liu, M.; Sun, Z. F.; Stram, A.; Mordaunt, A.; Velasco, J.; Ping, Y.; Zhang, Y.; Chen, S. W., *Nanowrinkled Carbon Aerogels Embedded with FeNx Sites as Effective Oxygen Electrodes for Rechargeable Zinc-Air Battery*; Research-China, 2019; Vol. *2019*, p 6813585.
(30) Arakawa, T.; Tomoto, K.; Nitta, H.; Toma, K.; Takeuchi, S.; Sekita, T.; Minakuchi, S.; Mitsubayashi, K. A Wearable Cellulose Acetate-Coated Mouthguard Biosensor for In Vivo Salivary Glucose Measurement. *Anal. Chem.* **2020**, *92*, 12201−12207.
(31) Han, J.; Li, M.; Li, H.; Li, C.; Ye, J.; Yang, B. Pt-poly(L-lactic acid) microelectrode-based microsensor for in situ glucose detection in sweat. *Biosens. Bioelectron.* **2020**, *170*, 112675.
(32) Lu, B.; Smart, T. J.; Qin, D.; Lu, J. E.; Wang, N.; Chen, L.; Peng, Y.; Ping, Y.; Chen, S. Nitrogen and Iron-Codoped Carbon Hollow Nanotubules as High-Performance Catalysts toward Oxygen Reduction Reaction: A Combined Experimental and Theoretical Study. *Chem. Mater.* **2017**, *29*, 5617−5628.
(33) He, T.; Lu, B.; Chen, Y.; Wang, Y.; Zhang, Y.; Davenport, J. L.; Chen, A. P.; Pao, C. W.; Liu, M.; Sun, Z.; Stram, A.; Mordaunt, A.; Velasco, J., Jr.; Ping, Y.; Zhang, Y.; Chen, S. *Nanowrinkled Carbon Aerogels Embedded with FeN x Sites as Effective Oxygen Electrodes for Rechargeable Zinc-Air Battery*; Research (Wash D C), 2019; Vol. *2019*, p 6813585.
(34) He, Y.; Li, X.; Xu, X.; Pan, J.; Niu, X. A cobalt-based polyoxometalate nanozyme with high peroxidase-mimicking activity at neutral pH for one-pot colorimetric analysis of glucose. *J. Mater. Chem. B* **2018**, *6*, 5750−5755.
(35) Alizadeh, N.; Salimi, A.; Hallaj, R.; Fathi, F.; Soleimani, F. CuO/WO3 nanoparticles decorated graphene oxide nanosheets with enhanced peroxidase-like activity for electrochemical cancer cell detection and targeted therapeutics. *Mater. Sci. Eng. C* **2019**, *99*, 1374−1383.
(36) Zhou, X.; Wang, M.; Chen, J.; Xie, X.; Su, X. Peroxidase-like activity of Fe-N-C single-atom nanozyme based colorimetric detection of galactose. *Anal. Chim. Acta* **2020**, *1128*, 72−79.
(37) Zhang, Y.; Lee, E. T.; Devereux, R. B.; Yeh, J.; Best, L. G.; Fabsitz, R. R.; Howard, B. V. Prehypertension, Diabetes, and Cardiovascular Disease Risk in a Population-Based Sample. *Hypertension* **2006**, *47*, 410−414.

https://doi.org/10.1021/acs.langmuir.1c01866
Langmuir 2021, 37, 11309−11315